8

Phase Shift Functions with Exponential Edge

The surface densities of heavy nuclei can be well represented by exponential functions. In fact, the function familiar from its role in the thermal Fermi distribution is widely used as an approximation in the description of densities of heavy nuclei. Such (Woods–Saxon) densities lead to phase shift functions that also have exponential edges. The present chapter is devoted to a survey of some properties of phase shift functions that have such an exponential edge. We have chosen to consider three examples,

$$\begin{aligned}\chi_{\exp}(b_x, b_y) &= A_{\exp}\, e^{-b/\beta} \\ &= A_{\exp} \exp\left(-\sqrt{b_x^2 + b_y^2}/\beta\right),\end{aligned} \tag{8.1}$$

$$\begin{aligned}\chi_{\cosh}(b_x, b_y) &= \frac{A_{\cosh}}{\cosh(b/\beta)} \\ &= \frac{A_{\cosh}}{\cosh\left(\sqrt{b_x^2 + b_y^2}/\beta\right)},\end{aligned} \tag{8.2}$$

$$\begin{aligned}\chi_{\mathrm{F}}(b_x, b_y) &= \frac{A_{\mathrm{F}}}{1 + \exp[(b - c)/\beta]} \\ &= \frac{A_{\mathrm{F}}}{1 + \exp\left[\left(\sqrt{b_x^2 + b_y^2} - c\right)/\beta\right]},\end{aligned} \tag{8.3}$$

which we shall refer to as the exponential, the inverse cosh, and the “Fermi” phase shift function, respectively.

In analogy with the comparison of phase shift functions with a Gaussian edge in Fig. 7.1, we also compare the three phase shift functions with an exponential edge in Fig. 8.1. For this purpose, we choose the relative normalizations

$$A_{\cosh} = A_{\exp}/2, \quad A_{\mathrm{F}} = A_{\exp}/\exp(c/\beta), \tag{8.4}$$

Downloaded from https://www.cambridge.org/core. IP address: 10.3.162.246, on 06 Dec 2025 at 15:30:57, subject to the Cambridge Core terms of use, available at https://www.cambridge.org/core/terms. https://doi.org/10.1017/9781316219256.011

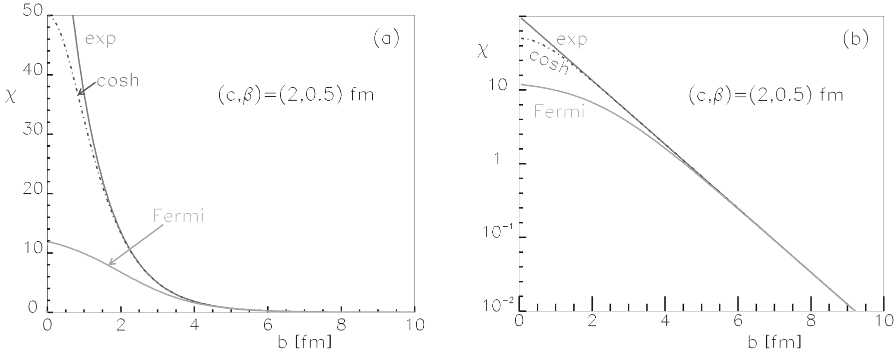

Figure 8.1 Phase shift functions Eqs. (7.1–7.3) with an exponential edge. The same three phase shift functions are shown both in linear (a) and logarithmic (b) representations.

and use the illustrative values $A_{\rm exp} = 100$, $c = 2$ fm, and $\beta = 0.5$ fm. At first sight (Fig. 8.1(a), where they are plotted linearly) they are rather different. However, in the case of strong absorption, it is the edge region which is important. This region is shown on a logarithmic scale, in Fig. 8.1(b). With the normalization of Eq. (8.4), the edge regions for these three phase shift functions are essentially the same in magnitude, as will be the envelopes of their patterns of oscillations.

Because of cylindrical symmetry, in the asymptotic approach we only need these phase shift functions for $b_y = 0$, and therefore define

$$
\begin{aligned}
X_{\rm exp}(b_x) &= A_{\rm exp}\, e^{-b_x/\beta}, \qquad\qquad \operatorname{Re} b_x > 0,\\
X_{\rm exp}(-b_x) &= X_{\rm exp}(b_x), \qquad\qquad (8.5)
\end{aligned}
$$

$$
X_{\rm cosh}(b_x) = \frac{A_{\rm cosh}}{\cosh(b_x/\beta)}, \qquad\qquad (8.6)
$$

$$
\begin{aligned}
X_{\rm F}(b_x) &= \frac{A_{\rm F}}{1 + \exp[(b_x - c)/\beta]}, \qquad \operatorname{Re} b_x > 0,\\
X_{\rm F}(-b_x) &= X_{\rm F}(b_x). \qquad\qquad (8.7)
\end{aligned}
$$

Since the pure exponential and the “Fermi” phase shift functions are not analytic at the origin, we need to give explicit definitions for $\operatorname{Re} b_x < 0$. Eqs. (8.5) and (8.7) correctly represent continuations of phase shift functions as even-valued in b_x. We can use these continuations as long as the stationary points do not get close to the origin.

In the case of the “Fermi” phase shift function, one can easily construct variations of Eq. (8.3) that are even and analytic at the origin. These include

Downloaded from https://www.cambridge.org/core. IP address: 10.3.162.246, on 06 Dec 2025 at 15:30:57, subject to the Cambridge Core terms of use, available at https://www.cambridge.org/core/terms. https://doi.org/10.1017/9781316219256.011

$$\tilde{\chi}_{\mathrm{F}}(b_x, b_y) = \frac{A}{\{1+\exp[(b-c)/\beta]\}\{1+\exp[(-b-c)/\beta]\}}, \tag{8.8}$$

and

$$\bar{\chi}_{\mathrm{F}}(b_x, b_y) = A\{[1+\exp[(-b-c)/\beta]]^{-1} + [1+\exp[(b-c)/\beta]]^{-1} - 1\}. \tag{8.9}$$

For large values of $|\boldsymbol{b}|/\beta$, i.e., at the nuclear surface, the three forms, Eqs. (8.1–8.3) have the same exponential behavior. As we shall see, for suitable choices of the parameters, and for small momentum transfers q, they therefore all lead to similar cross sections. However, their analytic properties in the complex b_x-plane are different (even disregarding the subtleties along the line $\operatorname{Re} b_x = 0$) and at sufficiently large momentum transfers the differential cross sections will therefore differ.

8.1 Evenness

Since we integrate over Cartesian coordinates b_x and b_y rather than cylindrical ones, we need to define the integrand carefully for negative values of b_x and b_y. The "Fermi" phase shift function Eq. (8.3) is for fixed b_y written as an even function of b_x. After integrating over b_y and evaluating the integrand for $b_y = 0$, the evenness is lost. The construction Eq. (8.7) is explicitly even in b_x, but it is not analytic at the origin. In fact, all odd derivatives are non-vanishing and opposite on the two sides. For the stationary-phase integration, this does not pose any problems, since the integrand is exponentially small near $b_x = 0$ and that region does not give any numerically significant contribution. The same is true for the exponential phase shift function, given by Eqs. (8.1) and (8.5).

For the direct numerical evaluation of the diffraction integral Eq. (7.29) in cylindrical coordinates, however, the distinction between Eqs. (8.3) and (8.8) is important at large momentum transfers. Without the evenness imposed by Eq. (8.8), the scattering amplitude would start to exhibit noise-like behavior at large momentum transfers.

8.2 Exponential Phase Shift Function

Consider first $X_{\exp}(b_x)$. The stationary points can be determined analytically as

$$b_{\alpha\, x} = \beta\left[-\log\left(\frac{|A_{\exp}|}{q\beta}\right) - i\varphi_A\right], \tag{8.10a}$$

$$b_{\beta\, x} = \beta\left[\log\left(\frac{|A_{\exp}|}{q\beta}\right) - i(\pi - \varphi_A)\right], \tag{8.10b}$$

Downloaded from https://www.cambridge.org/core. IP address: 10.3.162.246, on 06 Dec 2025 at 15:30:57, subject to the Cambridge Core terms of use, available at https://www.cambridge.org/core/terms. https://doi.org/10.1017/9781316219256.011

where

$$A_{\exp} \equiv |A_{\exp}|e^{i\varphi_A}. \tag{8.11}$$

Now, using the values of $X_{\exp}$ and $X''_{\exp}$ at the stationary points,

$$\begin{aligned} X_{\exp}(b_{\alpha\,x}) &= -X_{\exp}(b_{\beta\,x}) = q\beta, \\ X''_{\exp}(b_{\alpha\,x}) &= -X''_{\exp}(b_{\beta\,x}) = q/\beta, \end{aligned} \tag{8.12}$$

we obtain simple expressions for the corresponding amplitudes,

$$F = F(b_{\alpha\,x}) + F(b_{\beta\,x}), \tag{8.13}$$

with

$$F(b_{\alpha\,x}) = \frac{k}{iq}\sqrt{\beta b_{\alpha\,x}}\, e^{-iq(b_{\alpha\,x}-\beta)}, \tag{8.14a}$$

$$F(b_{\beta\,x}) = \frac{k}{iq}\sqrt{-\beta b_{\beta\,x}}\, e^{-iq(b_{\beta\,x}+\beta)}. \tag{8.14b}$$

The moduli of each of these will obviously fall as

$$|F(b_{\alpha\,x})| \sim e^{-q\beta\varphi_A}, \tag{8.15a}$$

$$|F(b_{\beta\,x})| \sim e^{-q\beta(\pi-\varphi_A)}. \tag{8.15b}$$

The different rates at which these fall off are thus simply given by the phase φ_A, and are equal for $\varphi_A = \pi/2$. Similarly, the period of oscillation in the cross section is given by

$$\begin{aligned} \Delta q &= \frac{\pi}{|\operatorname{Re}[b_{\alpha\,x} - b_{\beta\,x} - 2\beta]|} \\ &= \frac{\pi}{2\left[\log\left(\frac{|A_{\exp}|}{q\beta}\right) + \beta\right]}. \end{aligned} \tag{8.16}$$

Thus, we see that the asymptotic method provides us with simple and explicit formulas for the characteristics of the cross section.

In Fig. 8.2 we display the trajectories of the stationary points for $\varphi_A = 0^\circ$, 30°, 60°, and 90°. The arrows indicate the movement of the points of stationary phase, as the momentum transfer, q, is increased. Note that there is no rainbow singularity associated with $X_{\exp}(b_x)$ for $\varphi_A = 0^\circ$.

The cross sections corresponding to $\varphi_A = 30^\circ$ and 90° are shown in Figs. 8.3 and 8.4. Fig. 8.3 shows characteristic damping of the oscillations due to the different imaginary parts of the trajectories. Fig. 8.4 shows oscillations with increasing period as q increases as the two stationary points approach each other. Were the

Downloaded from https://www.cambridge.org/core. IP address: 10.3.162.246, on 06 Dec 2025 at 15:30:57, subject to the Cambridge Core terms of use, available at https://www.cambridge.org/core/terms. https://doi.org/10.1017/9781316219256.011

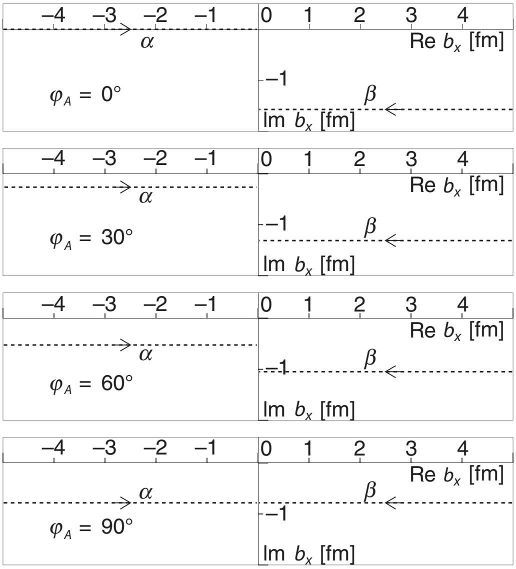

Figure 8.2 Trajectories of stationary points for the exponential phase shift function, $\chi_{\text{exp}} = A_{\text{exp}} \exp(-b/\beta)$. [Its definition for Cartesian coordinates, $\boldsymbol{b} = (b_x, b_y)$ is given by Eq. (8.1).] These trajectories are shown in the complex b_x-plane, the arrows indicate how they move with increasing q. (At the stationary points, $b_y = 0$.) Here $A_{\text{exp}} = |A_{\text{exp}}| \exp(i\varphi_A)$; four phases are considered, $\varphi_A = 0^\circ$, 30°, 60°, and 90°. Further, $\beta = 0.5$ fm. The present simple phase shift function, which is only an approximation to more realistic phase shift functions, has a discontinuous derivative along the line $\operatorname{Re} b_x = 0$. That line separates the two trajectories labeled α and β. For the case of pure absorption, the two trajectories satisfy $\operatorname{Im} b_{j\,x} = -\frac{1}{2}\pi\beta = -0.785$ fm.

imaginary parts of the stationary point coordinates the only parameters determining the slope of the envelope of the differential cross section, the envelope would have a constant slope on a logarithmic plot. The more slowly varying factors in the expression for the scattering amplitude are seen, on the contrary, to lead to a slight deviation from this constancy of slope.

8.3 Inverse cosh Phase Shift Function

Next, we consider $X_{\text{cosh}}(b_x)$ given by Eq. (8.6). Elementary algebra leads to explicit expressions for the stationary points. These take a simple form if we introduce the abbreviations

$$\lambda = \frac{A_{\text{cosh}}}{2q\beta}, \tag{8.17}$$

$$s_\pm = -\lambda \pm i\sqrt{1-\lambda^2}, \tag{8.18}$$

Downloaded from https://www.cambridge.org/core. IP address: 10.3.162.246, on 06 Dec 2025 at 15:30:57, subject to the Cambridge Core terms of use, available at https://www.cambridge.org/core/terms. https://doi.org/10.1017/9781316219256.011

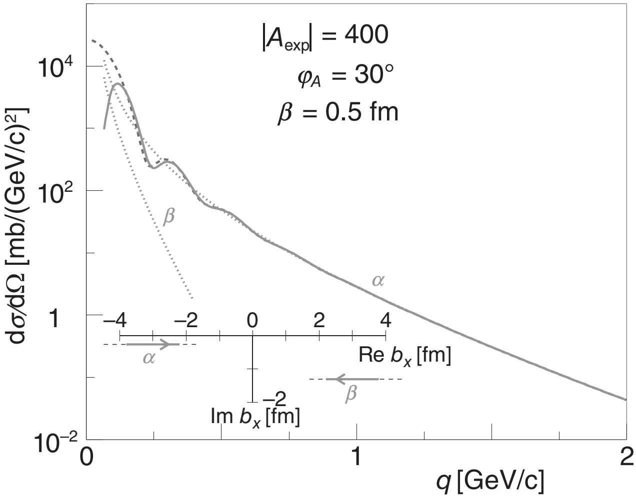

Figure 8.3 Differential cross section for $\chi_{\text{exp}}(b) = A_{\text{exp}} \exp(-b/\beta)$. Here $A_{\text{exp}} = |A_{\text{exp}}| \exp(i\varphi_A)$, with $|A_{\text{exp}}| = 400$. The phase shift function has a small absorptive part, $\varphi_A = 30^\circ$, and $\beta = 0.5$ fm. The inserts show the trajectories of stationary points for the range in momentum transfer 0.02 GeV/c $\leq q \leq$ 6.0 GeV/c (dotted). The parts of the trajectories that correspond to the cross-section plots, 0.05 GeV/c $\leq q \leq 2.0$ GeV/c, are indicated as solid curves. (The arrows indicate the sense in which the stationary points move as the momentum transfer increases.) The differential cross sections contributed by each of the stationary points, α and β, are shown as dotted curves. The solid curve shows the resulting cross section, evaluated in the asymptotic approach, whereas the dashed curve shows the result of a numerical evaluation of the diffraction integral, given by Eq. (2.2).

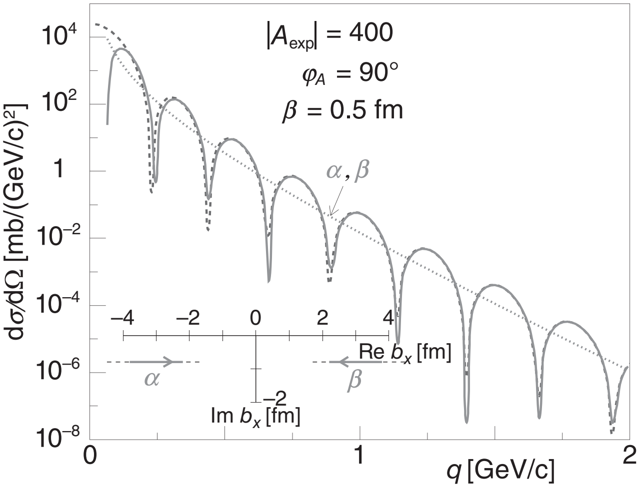

Figure 8.4 Similar to Fig. 8.3, for $\varphi_A = 90^\circ$.

Downloaded from https://www.cambridge.org/core. IP address: 10.3.162.246, on 06 Dec 2025 at 15:30:57, subject to the Cambridge Core terms of use, available at https://www.cambridge.org/core/terms. https://doi.org/10.1017/9781316219256.011

namely

$$b_{j\,x} = \beta \log\left[s_- \pm \sqrt{s_-^2 + 1}\right], \qquad j = \alpha, \beta, \tag{8.19a}$$

$$b_{j\,x} = \beta \left\{\log\left[s_+ \pm \sqrt{s_+^2 + 1}\right] - 2\pi i\right\}, \quad j = \gamma, \delta. \tag{8.19b}$$

Out of the infinite number of periodically repeating solutions, with period $2\pi i\beta$, we have selected those satisfying the inequality $-2\pi\beta < \operatorname{Im} b_{j\,x} \leq 0$ and through which the path of integration must be passed. For cases with absorption, only $b_{\alpha\,x}$ and $b_{\beta\,x}$ are relevant in this way, whereas for A_{cosh} real and positive (negative), $b_{\gamma\,x}$ ($b_{\delta\,x}$) will also be needed. For $\varphi_A = 0^\circ$, 30°, 60°, and 90°, these stationary points are shown in Fig. 8.5. The case $\varphi_A = 90^\circ$ corresponds to the function discussed in Section 5.1.

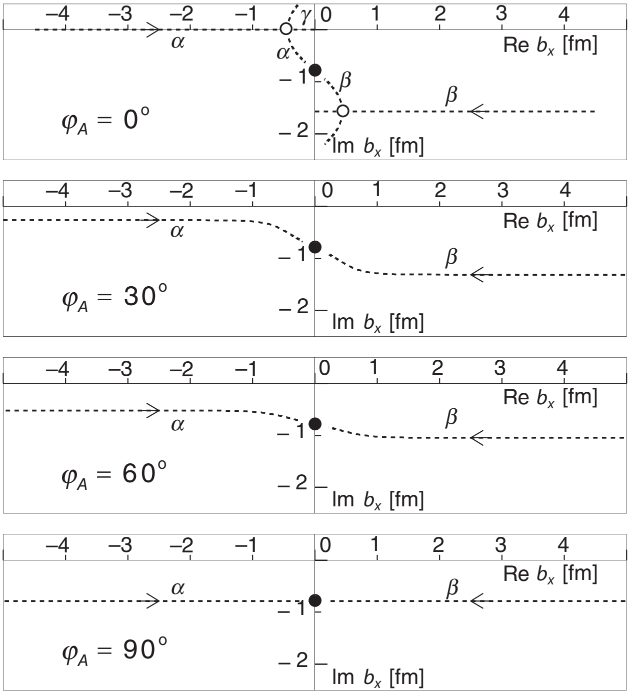

Figure 8.5 Trajectories of stationary points for $\chi_{\text{cosh}}(b) = A_{\text{cosh}}/\cosh(b/\beta)$, with $A_{\text{cosh}} = |A_{\text{cosh}}| \exp(i\varphi_A)$. These trajectories are shown in the complex b_x-plane, where $\boldsymbol{b} = (b_x, b_y)$. (At the stationary point, $b_y = 0$.) Four different phases are considered, $\varphi_A = 0^\circ, 30^\circ, 60^\circ$, and 90°, and $\beta = 0.5$ fm. The filled circles indicate poles of the phase shift function, whereas the open circles indicate zeros of its second derivative. One of these zeros, the one where for $\varphi_A = 0^\circ$ the trajectories α and γ run together, is a rainbow point. The other zero shown for $\varphi_A = 0^\circ$ (in the fourth quadrant) is not a rainbow point. In fact, neither the trajectory labeled β, nor its counterpart on the other side of the open circle, is encountered along the path of integration for $\varphi_A = 0^\circ$. (Compare the insert in Fig. 8.6.)

Downloaded from https://www.cambridge.org/core. IP address: 10.3.162.246, on 06 Dec 2025 at 15:30:57, subject to the Cambridge Core terms of use, available at https://www.cambridge.org/core/terms. https://doi.org/10.1017/9781316219256.011

Rainbow points can occur where

$$X''_{\cosh}(b_x) = -\frac{A_{\cosh}}{\beta^2}\frac{1-\sinh^2(b_x/\beta)}{\cosh^2(b_x/\beta)} = 0, \tag{8.20}$$

if $X'_{\cosh}(b_x)$ is simultaneously real and positive. These conditions are met for $A_{\cosh}$ real, and then correspond to

$$b_{x,\mathrm{R}} = -\beta \log(\sqrt{2}+1), \qquad \text{for } A_{\cosh} > 0, \tag{8.21a}$$

$$b_{x,\mathrm{R}} = \beta \log(\sqrt{2}+1), \qquad \text{for } A_{\cosh} < 0. \tag{8.21b}$$

The stationary point trajectories are seen to turn suddenly at right angles at the rainbow point (small circle) in Fig. 8.5. The rainbow singularity occurs for

$$q_{\mathrm{R}} = A_{\cosh}/2\beta. \tag{8.22}$$

In Fig. 8.6 we show the cross section for a real phase shift function with $A_{\cosh} = 10$ and $\beta = 0.5$ fm. A comparison with the exact evaluation of the diffraction

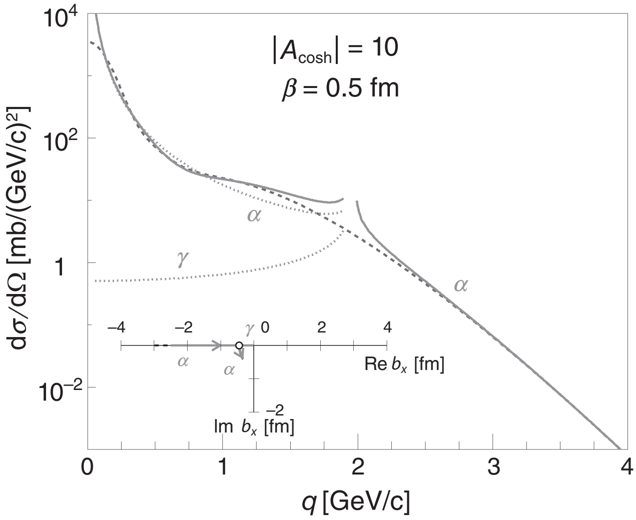

Figure 8.6 Differential cross sections for $\chi_{\cosh}(b) = A_{\cosh}/\cosh(b/\beta)$, with $A_{\cosh} = 10$ and $\beta = 0.5$ fm. The insert shows the trajectories of stationary points for the range in momentum transfers, 0.02 GeV/c $\le q \le 6.0$ GeV/c (dotted). The parts of the trajectories that correspond to the cross-section plot, 0.05 GeV/c $\le q \le 4.0$ GeV/c, are indicated as solid curves. (The arrows indicate the sense in which the stationary points move as the momentum transfer is increased.) As may be seen from a study of maps of the type given in Figs. 5.6 and 11.6, for a real, positive $A_{\cosh}$, the trajectory labeled β in Fig. 8.5 is not encountered along the path of integration. The differential cross sections contributed by each of the stationary points α and γ, are shown as dotted curves. The solid curve shows the resulting cross section, evaluated in the asymptotic approach (the spike represents the rainbow singularity), whereas the dashed curve shows the result of a numerical evaluation of the diffraction integral.

Downloaded from https://www.cambridge.org/core. IP address: 10.3.162.246, on 06 Dec 2025 at 15:30:57, subject to the Cambridge Core terms of use, available at https://www.cambridge.org/core/terms. https://doi.org/10.1017/9781316219256.011

integral shows that the agreement is excellent, apart from small intervals close to $q = 0$ and $q = q_R$. These features are quite analogous to those encountered for the real Gaussian phase shift function. (Compare Fig. 7.3 and the corresponding discussion in Chapter 7.)

Consider for a moment parameters $A_{\cosh}$, β, and a range in q such that

$$|\lambda| \equiv \frac{|A_{\cosh}|}{2q\beta} \gg 1. \tag{8.23}$$

We then have

$$b_{\alpha x} \simeq \beta\left[-\log\left(\frac{2|A_{\cosh}|}{q\beta}\right) - i\varphi_A\right], \tag{8.24a}$$

$$b_{\beta x} \simeq \beta\left[\log\left(\frac{2|A_{\cosh}|}{q\beta}\right) - i(\pi - \varphi_A)\right], \tag{8.24b}$$

which for $2A_{\cosh} = A_{\exp}$ are the same as for the exponential case, Eq. (8.10). In this limit, we also find that $X_{\cosh}(b_{jx})$ and $X''_{\cosh}(b_{jx})$ are equal to $X_{\exp}(b_{jx})$ and $X''_{\exp}(b_{jx})$, respectively. It follows that in the range of momentum transfers satisfying Eq. (8.23), one cannot distinguish between $X_{\exp}(b_x)$ and $X_{\cosh}(b_x)$.

Let us now turn to a discussion of weaker interactions or larger momentum transfers, such that

$$|\lambda| \equiv \frac{|A_{\cosh}|}{2q\beta} \ll 1. \tag{8.25}$$

Neglecting terms of order $|\lambda|$, we find from Eqs. (8.18) and (8.19) that

$$b_{jx} \simeq \beta\left[\pm(-1+i)\left(\frac{|A_{\cosh}|}{2q\beta}\right)^{\frac{1}{2}} e^{i\varphi_A/2} - \frac{i\pi}{2}\right], \quad j = \alpha, \beta. \tag{8.26}$$

Thus

$$\operatorname{Re} b_{jx} \simeq \mp\beta\left(\frac{|A_{\cosh}|}{2q\beta}\right)^{\frac{1}{2}}\left(\cos\frac{\varphi_A}{2} + \sin\frac{\varphi_A}{2}\right), \tag{8.27}$$

and

$$\operatorname{Im} b_{jx} \simeq -\beta\left[\frac{\pi}{2} \mp \left(\frac{|A_{\cosh}|}{2q\beta}\right)^{\frac{1}{2}}\left(\cos\frac{\varphi_A}{2} - \sin\frac{\varphi_A}{2}\right)\right]. \tag{8.28}$$

In this regime, the period of oscillation will increase as

$$\begin{aligned}\Delta q &= \frac{\pi}{\left|\operatorname{Re}\left\{b_{\alpha x} - b_{\beta x} - \frac{1}{q}\left[X(b_{\alpha x}) - X(b_{\beta x})\right]\right\}\right|}\\ &= \frac{\pi}{\beta}\left(\frac{2q\beta}{|A_{\cosh}|}\right)^{\frac{1}{2}} \Big/ \left(\cos\frac{\varphi_A}{2} + \sin\frac{\varphi_A}{2}\right),\end{aligned} \tag{8.29}$$

which is much faster than the logarithmic behavior found for $|\lambda| \gg 1$. Also, the rate at which the modulus of each term, $|F(b_{\alpha x})|$ and $|F(b_{\beta x})|$, decreases

Downloaded from https://www.cambridge.org/core. IP address: 10.3.162.246, on 06 Dec 2025 at 15:30:57, subject to the Cambridge Core terms of use, available at https://www.cambridge.org/core/terms. https://doi.org/10.1017/9781316219256.011

[cf. Eq. (8.28)], is different from what it was for $|\lambda| \gg 1$. In particular, both slopes tend to the same value, $-\pi\beta/2$, as $q \to \infty$, independent of φ_A. This is of course dictated by the singularity at $b_x = -i\pi\beta/2$. Their difference vanishes like $q^{-1/2}$.

This type of behavior is illustrated in Fig. 8.7, where we have plotted $\mathrm{d}\sigma/\mathrm{d}\Omega$ corresponding to $|A_{\cosh}| = 5$, $\varphi_A = 75°$ and $90°$, $\beta = 0.5$ fm. As in Chapter 7, we have adopted the value of the momentum as $k = 1.7$ GeV/c, corresponding

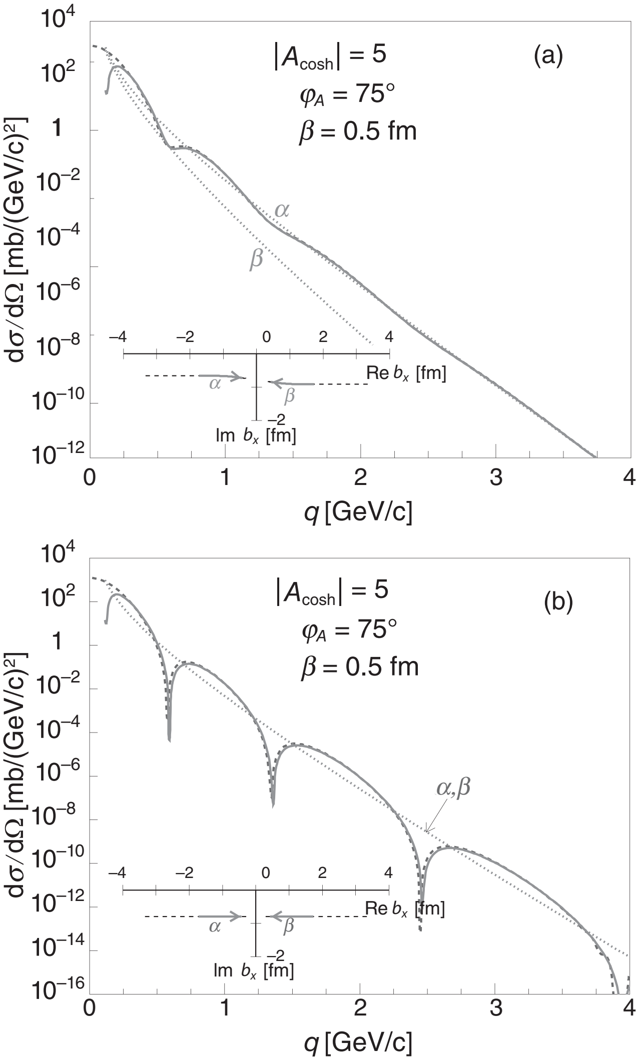

Figure 8.7 Differential cross sections for $\chi_{\cosh}(b) = A_{\cosh}/\cosh(b/\beta)$, with $A_{\cosh} = |A_{\cosh}|\exp(i\varphi_A)$, $|A_{\cosh}| = 5$, and $\beta = 0.5$ fm. Two cases are considered, (a) $\varphi_A = 75°$, and (b) $\varphi_A = 90°$. The individual contributions of the two stationary points (see inserts) are shown as dotted curves, whereas the resulting interference patterns are shown by the solid curves. The dashed curves give the results of numerical evaluations of the diffraction integrals.

Downloaded from https://www.cambridge.org/core. IP address: 10.3.162.246, on 06 Dec 2025 at 15:30:57, subject to the Cambridge Core terms of use, available at https://www.cambridge.org/core/terms. https://doi.org/10.1017/9781316219256.011

to $T_{\text{kin}} = 1$ GeV. The value of $|\lambda|$ for this case ranges between 0.99 and 0.25 for q in the interval $1\ \text{GeV/c} \leq q \leq 4\ \text{GeV/c}$. In Fig. 8.7a the differential cross section for $\varphi_A = 75^\circ$ shows a sequence of damped oscillations of a sort frequently encountered in diffraction patterns. The oscillations are of course produced by the interference of the amplitudes contributed by the stationary points labeled α and β. The damping of the oscillations occurs because the two trajectories yield stationary points which have different imaginary parts. The scattered intensity for large q is given almost entirely by the squared modulus of the amplitude corresponding to $b_{\alpha x}$. In Fig. 8.7b, corresponding to a purely imaginary interaction, $\varphi_A = 90^\circ$, the oscillations are undamped, since the two trajectories have equal imaginary parts. In both Figs. 8.7a and 8.7b, a lengthening of the period of oscillation is evident as q increases, since the distance between the stationary points decreases. Both graphs show excellent agreement between the asymptotic theory and the exact evaluation of the diffraction integral.

8.4 "Fermi" Phase Shift Function

The third example of a phase shift function with exponential edge is the "Fermi" form, Eq. (8.7). This differs from the previous two by possessing one more shape parameter, the radius c. As in the two previous cases, the stationary point can once more be determined analytically. As an abbreviation, let us introduce

$$\lambda \equiv \frac{A_{\text{F}}}{2q\beta}. \tag{8.30}$$

The stationary points are then given in terms of c, β, and λ for $\varphi_A > 0$ by

$$b_{\alpha x} = -c - i\pi\beta - \beta \log\left[1 - \lambda + \sqrt{(1-\lambda)^2 - 1}\right], \tag{8.31a}$$

$$b_{\beta x} = c - i\pi\beta + \beta \log\left[1 + \lambda + \sqrt{(1+\lambda)^2 - 1}\right]. \tag{8.31b}$$

Similarly, for $\varphi_A = 0^\circ$, we find

$$b_{\alpha x} = -c - i\pi\beta - \beta \log\left[1 - \lambda - i\sqrt{2\lambda - \lambda^2}\right], \tag{8.32a}$$

$$b_{\beta x} = c - i\pi\beta + \beta \log\left[1 + \lambda + \sqrt{2\lambda - \lambda^2}\right], \tag{8.32b}$$

$$b_{\gamma x} = -c + i\pi\beta - \beta \log\left[1 - \lambda + i\sqrt{2\lambda - \lambda^2}\right]. \tag{8.32c}$$

In these expressions, as well as in Eq. (8.31), the signs in front of the square roots correspond to the solutions that are relevant for $|\lambda| \to 0$. For large values of $|\lambda|$,

Downloaded from https://www.cambridge.org/core. IP address: 10.3.162.246, on 06 Dec 2025 at 15:30:57, subject to the Cambridge Core terms of use, available at https://www.cambridge.org/core/terms. https://doi.org/10.1017/9781316219256.011

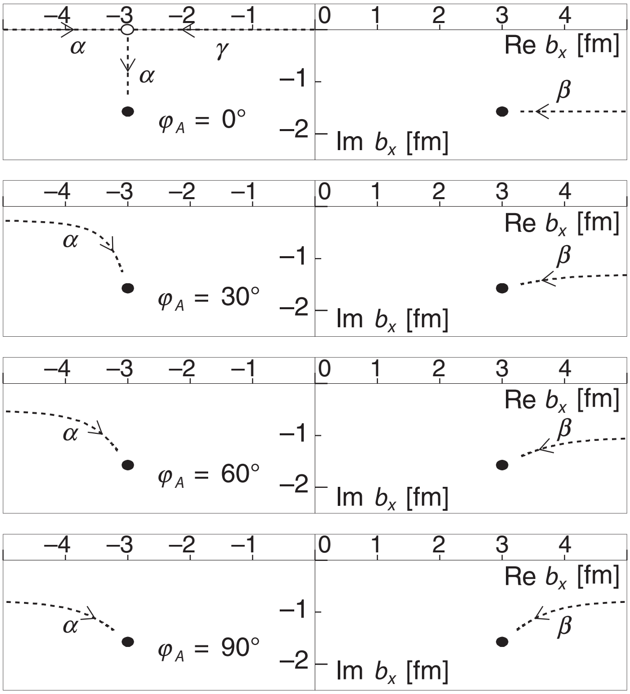

Figure 8.8 Trajectories of stationary points for the "Fermi" phase shift function, $\chi_{\mathrm{F}}(b) = A_{\mathrm{F}}/\{1+\exp[(b-c)/\beta]\}$. These trajectories are shown in the complex b_x-plane, where $\boldsymbol{b} = (b_x, b_y)$. (At the stationary points, $b_y = 0$.) Again four different phases are considered, $\varphi = 0°, 30°, 60°$, and $90°$. The radius and surface thickness parameters are: $c = 3$ fm and $\beta = 0.5$ fm. The filled circles indicate poles of the phase shift function (at $b_x = \pm c - i\pi\beta$), and the open circle (for $\varphi = 0°$) indicates a rainbow point (at $b_x = -c$).

these square roots, as well as the logarithms, must be continued in an analytic fashion, starting with $|\lambda| < 1$.

Asymptotically, as $q \to \infty$, $|\lambda| \to 0$ and

$$b_{\alpha\, x} \simeq -c - i\pi\beta + i\beta e^{i\varphi_A/2}\left(\frac{|A_{\mathrm{F}}|}{q\beta}\right)^{1/2}, \tag{8.33a}$$

$$b_{\beta\, x} \simeq c - i\pi\beta + \beta e^{i\varphi_A/2}\left(\frac{|A_{\mathrm{F}}|}{q\beta}\right)^{1/2}, \tag{8.33b}$$

i.e., they approach the poles of $X'_{\mathrm{F}}(b_x)$.

Trajectories of the stationary points corresponding to $c = 3$ fm, $\beta = 0.5$ fm, and $\varphi_A = 0°, 30°, 60°$, and $90°$ are given in Fig. 8.8. One may note that, as $q \to \infty$, the poles are approached from different directions, depending on φ_A [cf. Eq. (8.33)].

For small momentum transfers ($|\lambda| \gg 1$), the stationary points are well approximated by

Downloaded from https://www.cambridge.org/core. IP address: 10.3.162.246, on 06 Dec 2025 at 15:30:57, subject to the Cambridge Core terms of use, available at https://www.cambridge.org/core/terms. https://doi.org/10.1017/9781316219256.011

$$b_{\alpha x} = -c - \beta \log\left(\frac{|A_{\mathrm{F}}|}{q\beta}\right) - i\beta\varphi_A, \tag{8.34a}$$

$$b_{\beta x} = c + \beta \log\left(\frac{|A_{\mathrm{F}}|}{q\beta}\right) - i\beta(\pi - \varphi_A). \tag{8.34b}$$

In this limit, they will coincide with those for X_{exp} [cf. Eq. (8.10)] provided

$$A_{\mathrm{F}} = A_{\mathrm{exp}}\, e^{-c/\beta}. \tag{8.35}$$

At the stationary point, the phase shift function and its second derivative may be written as

$$X_{\mathrm{F}}(b_{\alpha x}) = \tfrac{1}{2}A_{\mathrm{F}} - i[A_{\mathrm{F}}\, q\beta - \tfrac{1}{4}{A_{\mathrm{F}}}^2]^{1/2}, \tag{8.36a}$$

$$X_{\mathrm{F}}(b_{\beta x}) = \tfrac{1}{2}A_{\mathrm{F}} - [A_{\mathrm{F}}\, q\beta + \tfrac{1}{4}{A_{\mathrm{F}}}^2]^{1/2}, \tag{8.36b}$$

and

$$X''_{\mathrm{F}}(b_{\alpha x}) = \frac{q}{\beta}\left[1 - 2\frac{X_{\mathrm{F}}(b_{\alpha x})}{A_{\mathrm{F}}}\right], \tag{8.37a}$$

$$X''_{\mathrm{F}}(b_{\beta x}) = -\frac{q}{\beta}\left[1 - 2\frac{X_{\mathrm{F}}(b_{\beta x})}{A_{\mathrm{F}}}\right]. \tag{8.37b}$$

It is now easily seen that when $q\beta/|A_{\mathrm{F}}| \ll 1$, and if Eq. (8.35) is fulfilled, the cross section will be the same as for X_{exp}. This is yet another example of how the asymptotic method allows us to determine quantitatively when phase shift functions with similar edges yield cross sections which are quite different in form. In the present examples, such differences indeed occur for $q\beta/|A_{\mathrm{F}}| \gtrsim 1$ and are illustrated in Fig. 8.12.

For large values of $q\beta/|A_{\mathrm{F}}|$, it follows from Eq. (8.36) that

$$X_{\mathrm{F}}(b_{\alpha x}) \simeq -i e^{i\varphi_A/2}[q\beta|A_{\mathrm{F}}|]^{1/2}, \tag{8.38a}$$

$$X_{\mathrm{F}}(b_{\beta x}) \simeq -e^{i\varphi_A/2}[q\beta|A_{\mathrm{F}}|]^{1/2}. \tag{8.38b}$$

Thus, the modulus of each term will fall for large q in a nearly exponential fashion,

$$|F(b_{\alpha x})| \sim \exp\left\{-q\beta\left[\pi - 2\cos\left(\frac{\varphi_A}{2}\right)\left(\frac{|A_{\mathrm{F}}|}{q\beta}\right)^{1/2}\right]\right\}, \tag{8.39a}$$

$$|F(b_{\beta x})| \sim \exp\left\{-q\beta\left[\pi - 2\sin\left(\frac{\varphi_A}{2}\right)\left(\frac{|A_{\mathrm{F}}|}{q\beta}\right)^{1/2}\right]\right\}, \tag{8.39b}$$

Downloaded from https://www.cambridge.org/core. IP address: 10.3.162.246, on 06 Dec 2025 at 15:30:57, subject to the Cambridge Core terms of use, available at https://www.cambridge.org/core/terms. https://doi.org/10.1017/9781316219256.011

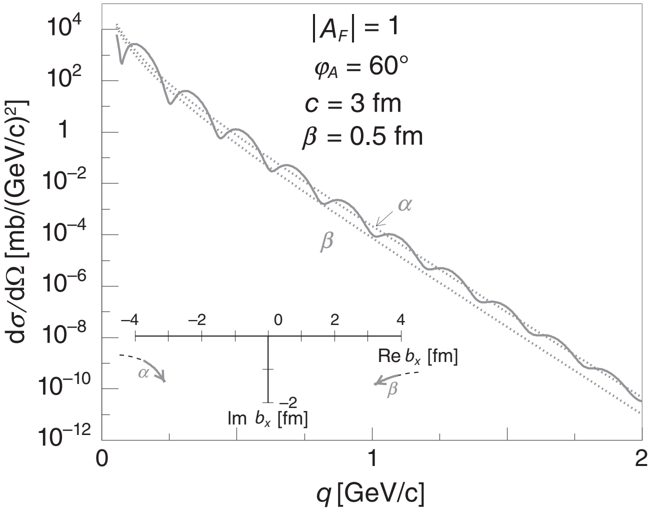

Figure 8.9 Differential cross section for the “Fermi” phase shift function, $\chi_{\mathrm{F}}(b) = A_{\mathrm{F}}/\{1 + \exp[(b - c)/\beta]\}$, with $A_{\mathrm{F}} = |A_{\mathrm{F}}| \exp(i\varphi_A)$. Here $|A_{\mathrm{F}}| = 1$, $c = 3$ fm, and $\beta = 0.5$ fm. A significant degree of absorption is considered, $\varphi_A = 60°$. The inserts show the trajectories of stationary points for the range in momentum transfer, 0.02 GeV/c $\leq q \leq$ 6.0 GeV/c (dotted). The parts of the trajectories that correspond to the cross section plots, 0.05 GeV/c $\leq q \leq$ 2.0 GeV/c, are indicated as solid curves. The differential cross sections contributed by each of the stationary points, α and β, are indicated by dotted curves. The solid curve shows the resulting cross section, evaluated in the asymptotic approach, whereas the dashed curve shows the result of a numerical evaluation of the diffraction integral.

and the period of oscillation will approach its constant asymptotic value, $\pi/2c$ in a similar fashion

$$\Delta q \simeq \frac{\pi}{2\left[c + \beta\left(\cos\frac{\varphi_A}{2} + \sin\frac{\varphi_A}{2}\right)\left(\frac{|A_{\mathrm{F}}|}{q\beta}\right)^{1/2}\right]}. \tag{8.40}$$

We note that the asymptotic period is approached from below.

In Figs. 8.9 and 8.10 we show cross sections corresponding to X_{F} for $|A_{\mathrm{F}}| = 1$, $c = 3$ fm, and $\beta = 0.5$ fm. In Fig. 8.9 $\varphi_A = 60°$ while in Fig. 8.10 $\varphi_A = 90°$ and X_{F} is purely imaginary. For the latter case the choice of parameters is roughly appropriate to proton–calcium scattering at 1 GeV. These graphs show two features that are frequently noted as approximate qualities of scattering by heavy nuclei. Their envelopes have nearly constant logarithmic slopes and their periods of oscillation are nearly constant as well. The reason for this behavior of the calculated cross sections lies in the pole singularity of the function X_{F} given by Eq. (8.1). As the momentum transfer q increases to larger values, the stationary points labeled α and β approach the poles of X_{F} [see Eq. (8.33)]. In fact, they approach the poles

Downloaded from https://www.cambridge.org/core. IP address: 10.3.162.246, on 06 Dec 2025 at 15:30:57, subject to the Cambridge Core terms of use, available at https://www.cambridge.org/core/terms. https://doi.org/10.1017/9781316219256.011

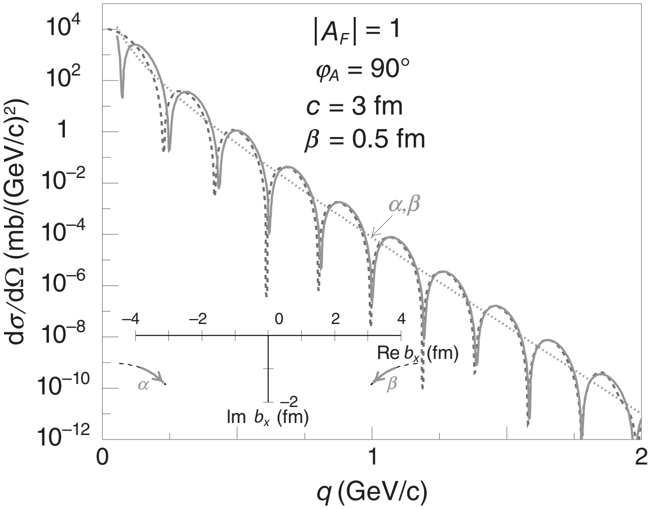

Figure 8.10 Similar to Fig. 8.9, for $\varphi_A = 90°$.

closely for modest values of q and then hardly move at all as q increases. The effect of the poles of X_F then is to stabilize the slope and the oscillation period of the corresponding elastic differential cross section.

Once again, characteristically, the cross section oscillations for the purely imaginary interaction, Fig. 8.10, are undamped, while those for the complex interaction, Fig. 8.9, are damped. From these and our earlier results it is clear that the presence of undamped oscillations in a logarithmic plot of a differential cross section indicates that the interaction is greatly dominated by the imaginary or absorptive part. Another characteristic of purely absorptive interactions is that within the context of diffraction theory the differential cross sections have periodic zeros. Corrections to the diffraction theory, Coulomb field effects, and various spin-dependent effects will tend to fill in the zeros, however, and leave minima that are often considerably less pronounced. Figs. 8.9 and 8.10 both indicate that the asymptotic theory is fairly accurate away from the forward direction for the "Fermi" phase shift function. Actually, the result of the numerical evaluation of the diffraction integral is based on the symmetrized phase shift function, Eq. (8.8). Without such a symmetry (or evenness, see Section 8.1), the cross section would start to deviate from this regular pattern around $q = 1.5$ GeV/c.

As is seen from Eq. (8.31), the stationary points depend on the strength of the interaction through the parameter $\lambda = A_\mathrm{F}/2q\beta$. On the other hand, $X_\mathrm{F}(b_{jx})$ and $X''_\mathrm{F}(b_{jx})$ are functions of both A_F and λ, and thus the cross section will depend on A_F and λ separately. As a result, the period of oscillation of the differential cross section and the slope of its envelope will depend not only on c and β, but on the

Downloaded from https://www.cambridge.org/core. IP address: 10.3.162.246, on 06 Dec 2025 at 15:30:57, subject to the Cambridge Core terms of use, available at https://www.cambridge.org/core/terms. https://doi.org/10.1017/9781316219256.011

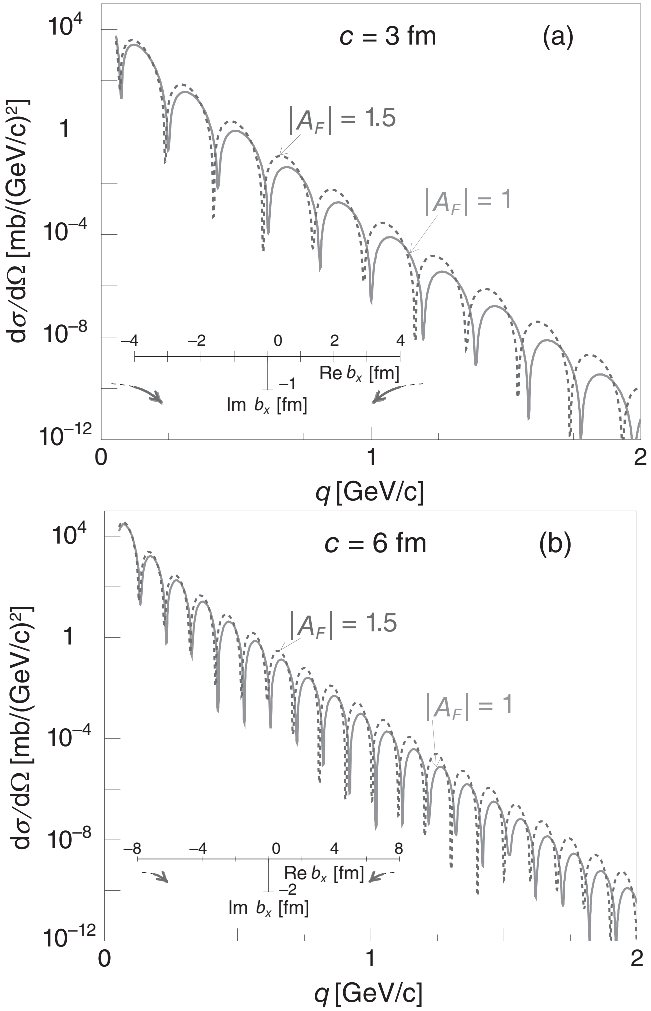

Figure 8.11 Differential cross sections for the “Fermi” phase shift function, $\chi_F(b) = A_F/\{1 + \exp[(b - c)/\beta]\}$. Two radius parameters are considered, (a) $c = 3$ fm, (b) $c = 6$ fm. In both cases, $\beta = 0.5$ fm and A_F is purely imaginary. The figure illustrates the fact that not only the geometry, but also the strength of the interaction is of importance for the shape of the differential cross section.

magnitude of A_F as well. This dependence is illustrated in Fig. 8.11 for interactions of two different radii. Increasing the strength of the interaction is seen to decrease the oscillation period of the cross section. The same dependence is evident in our earlier Fig. 7.7.

We have seen that at small momentum transfers three different phase shift functions, X_{exp}, X_{cosh}, and X_F may lead to the same cross section. Obviously, at sufficiently large momentum transfer, one may distinguish between them. This is

Downloaded from https://www.cambridge.org/core. IP address: 10.3.162.246, on 06 Dec 2025 at 15:30:57, subject to the Cambridge Core terms of use, available at https://www.cambridge.org/core/terms. https://doi.org/10.1017/9781316219256.011

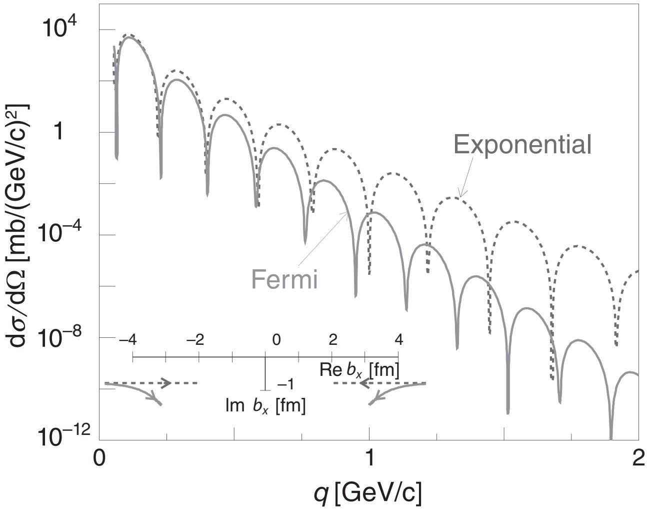

Figure 8.12 A comparison of the differential cross sections resulting from two phase shift functions that coincide at large parameters, but that are different in the interior, $\chi_{\text{exp}}(b) = A_{\text{exp}} \exp(-b/\beta)$ (dashed), and $\chi_{\text{F}}(b) = A_{\text{F}}/\{1 + \exp[(b - c)/\beta]\}$ (solid). The parameters satisfy Eq. (8.35). Further, $c = 3$ fm, $\beta = 0.5$ fm, and $A_{\text{F}} = 2i$. The trajectories of stationary points are given in the insert.

illustrated in Fig. 8.12, where we compare the cross sections corresponding to X_{exp} and X_{F}, for parameters satisfying Eq. (8.35), and with $c = 3$ fm, $\beta = 0.5$ fm, and $A_{\text{F}} = 2i$. We see that the oscillations in the cross sections corresponding to X_{F} and X_{exp} start to get out of phase and differ in slope when

$$q \gtrsim \frac{|A_{\text{F}}|}{2\beta}, \tag{8.41}$$

which corresponds to $q \gtrsim 0.4\,\text{GeV/c}$. (A similar comparison between X_{exp} and X_{cosh}, with $A_{\text{exp}} = 2A_{\text{cosh}}$, would lead to an agreement between the two out to $q \leq |A_{\text{cosh}}|/2\beta$.)

We conclude this section with a comparison of the potentials corresponding to the phase shift functions studied in Fig. 8.12. These are easily determined numerically from Eq. (2.6a). As shown in Fig. 8.13, for a choice of parameters satisfying Eq. (8.35), they are quite similar at large values of r, but differ greatly for smaller radii.

For applications to proton–nucleus scattering, one often considers an optical potential proportional to a Woods–Saxon density function ρ_{WS}. If we assume a proportionality between the optical potential and the density, then the density, $\rho[T_{\text{F}}]$ corresponding to a "Fermi" thickness function,[1] $T_{\text{F}}(b)$ is readily determined

---

[1] If the range of interaction can be neglected, this is equivalent to a "Fermi" phase shift function, $\chi_{\text{F}}(b_x, b_y)$.

Downloaded from https://www.cambridge.org/core. IP address: 10.3.162.246, on 06 Dec 2025 at 15:30:57, subject to the Cambridge Core terms of use, available at https://www.cambridge.org/core/terms. https://doi.org/10.1017/9781316219256.011

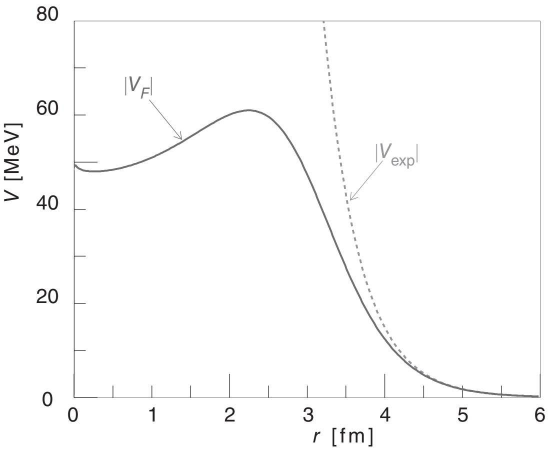

Figure 8.13 Moduli of the potentials corresponding to the exponential and “Fermi” phase shift functions considered in Fig. 8.12.

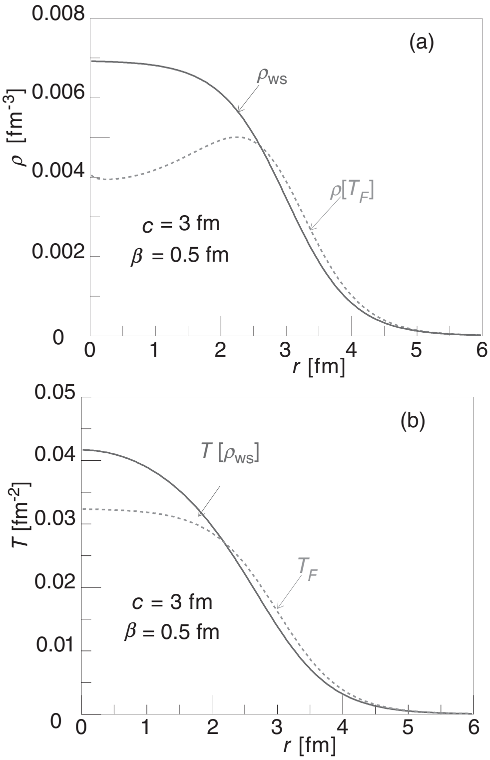

Figure 8.14 (a) A comparison of the Woods–Saxon density, $\rho_{\mathrm{WS}}(r) = \rho_0/\{1 + \exp[(r-c)/\beta]\}$, with the density corresponding to the “Fermi” phase shift function (or a “Fermi” thickness function), $\rho[T_{\mathrm{F}}]$. The normalization is $\int \mathrm{d}^3 r \rho(r) = 1$. The shape parameters, c and β, are the same in both cases. (b) A comparison of the thickness function corresponding to the Woods–Saxon density, $T[\rho_{\mathrm{WS}}]$, with the “Fermi” thickness function, $T_{\mathrm{F}} = T_0/\{1 + \exp[(b-c)/\beta]\}$. The normalization is $\int \mathrm{d}^2 b T(b) = 1$. Again the shape parameters are the same.

Downloaded from https://www.cambridge.org/core. IP address: 10.3.162.246, on 06 Dec 2025 at 15:30:57, subject to the Cambridge Core terms of use, available at https://www.cambridge.org/core/terms. https://doi.org/10.1017/9781316219256.011

from the Abel integral equation, Eq. (2.6c). These densities (both normalized to $\int d^3r\rho(r) = 1$) are compared in Fig. 8.14a for $c = 3$ fm and $\beta = 0.5$ fm. For $r \gtrsim c$ (i.e., in the region that is most significant in determining the cross section) they are rather similar in shape, but differ somewhat in normalization. We also note that $\rho[T_\mathrm{F}]$ has an enhancement in the region of the surface. Since such an enhancement is sometimes encountered in shell-model calculations [4,18] of nuclear densities, there could be instances in which $\rho[T_\mathrm{F}]$ better represents the nuclear density than ρ_WS.

For completeness, we also compare in Fig. 8.14b the corresponding thickness functions, $T[\rho_\mathrm{WS}]$ and T_F, which are quantities more closely related to the cross section. The fact that these are more similar than the densities from which they are derived indicates one reason why nuclear cross sections depend only weakly on the behavior of the density function at small radii.

Downloaded from https://www.cambridge.org/core. IP address: 10.3.162.246, on 06 Dec 2025 at 15:30:57, subject to the Cambridge Core terms of use, available at https://www.cambridge.org/core/terms. https://doi.org/10.1017/9781316219256.011